Article type: Communication

Enhancement of the Performance of Perovskite Solar Cells, LEDs and Optical Amplifiers by Anti-Solvent Additive Deposition

Thi Tuyen Ngo, Isaac Suarez, Gabriella Antonicelli, Diego Cortizo-Lacalle, Juan P. Martinez-Pastor,* Aurelio Mateo-Alonso* and Ivan Mora-Sero*

Thi Tuyen Ngo, Ass. Prof. Ivan Mora-Sero
Institute of Advanced Materials (INAM), UniversitatJaume I, 12006 Castelló, Spain.
E-mail: sero@uji.es
Dr. Isaac Suárez, Prof. Juan P. Martínez-Pastor
UMDO, Instituto de Ciencia de los Materiales, Universidad de Valencia, 46071 Valencia, Spain.
E-mail: Juan.Mtnez.Pastor@uv.es
Gabriella Antonicelli, Dr. Diego Cortizo-Lacalle, Prof. Aurelio Mateo-Alonso
POLYMAT, University of the Basque Country UPV/EHU, Avenida de Tolosa 72, E-20018 Donostia-San Sebastian, Spain. Email: amateo@polymat.eu
Prof. Aurelio Mateo-Alonso
Ikerbasque, Basque Foundation for Science, E-48011 Bilbao, Spain

Halide Perovskites (PS) have emerged as an outstanding material family for optoelectronic applications[1] because of their superior physical properties, such as high optical absorption coefficients,[2] benign defect physics,[3] long and balanced electron–hole diffusion lengths,[4] good charge transport properties even in polycrystalline films,[1a] and low non-radiative recombination.[5] Photoconversion efficiency has reached 22.1%[6] a few years after the first reports on PS based liquid electrolyte solar cells in 2009.[7] Besides the application in photovoltaics, PS have been successfully employed in light emitting diodes (LED),[8] optical amplifiers,[9] and lasers.[10] In addition, the success of these materials mainly lies in that high efficiency devices are prepared with PS polycrystalline films that can be grown using solution methods[5c, 11] at low processing temperatures and, consequently, using low cost fabrication techniques. Furthermore, these growth techniques allow the easy combination of PS with

other materials, as for example PbS quantum dots,[12] that induce interesting synergies. This fact opens a broad range of possibilities for the interaction of PS with organic compounds beyond their use as selective contacts.[13] Organic compounds are appealing materials for electronic applications since an unlimited number of structures can be potentially synthesized and they are relatively easy to design and/or modify to meet the requirements of specific applications.

The passivation of PS plays a crucial role in the efficiency of PS-based devices as it has been shown that the presence of electron traps favours faster non-radiative decays, while long carrier lifetimes and high photoluminescence efficiencies are in general indicators of better performing PS layers. Exposure of PS films to electron deficient aromatic compounds such as pyridine[14] and PCBM[15] have resulted in enhanced efficiencies associated to the passivation of such electron traps. Among the myriad of different electron deficient aromatic compounds, nitrogen-containing polycyclic aromatic hydrocarbons (N-PAHs)[16] have recently reemerged as a platform for developing small molecule n-type semiconductors that have been able to compete with fullerenes in several applications.[17] In particular, N-PAHs containing pyrazine rings have attracted much attention as they combine a series of optimal optoelectronic and electric properties that can further tuned thanks to the recent development of straightforward and solid synthetic routes.[16]

We have developed a new method to introduce additives *in situ* in a halide perovskite thin film, during the anti-solvent deposition step.[11b, 11c, 18] Solar cell, LED and waveguide optical amplifier devices have been prepared using the perovskite layer, concretely $CH_3NH_3PbI_3$, mixed separately with two different electron deficient heteroatom-doped PAHs, namely a twisted hexaazatrinaphthylene (HATNA)[16i, 19] and a bisthiadiazole-fusedtetraazapentacenequinone (DCL97)[20] (Figure 1). We have selected these two compounds among others as: i) they are novel compounds with different functionalities, that have not been previously checked for passivation in perovskite optoelectronic devices; ii) they

2

contain PAHs, that it has been reported to be excellent passivation agents,[14-15] displaying electrochemical LUMOs (or electron affinities) in the range of those observed for fullerene derivatives with excellent results for passivation;[15] iii) they possess different but complementary electronic absorption spectra that allow the selective excitation for characterization purposes and also investigating if their absorption features might also play a role under illumination; iv) they are soluble and chemically stable in the anti-solvents required for the fabrication of the devices.

With both molecules, we have observed a significant improvement of the performance of PS-based solar cell, LED and waveguide optical amplifier devices. Photoconversion efficiency of solar cells has been increased with respect to a reference cell, with no additives, while current/potential hysteresis decreased and solar cell stability increased. We have also observed an increase of the external quantum efficiency (EQE) for PS LEDs by a factor of 2-4 and the reduction of the light amplification threshold energy by a factor of 2-4 when organic additives are used. A systematic characterization of $CH_3NH_3PbI_3$ with additives points to a reduction in the non-radiative carrier recombination paths by the passivation of PS interface and grain boundaries in the polycrystalline film. They main scope of this work is to present a general method in order to increase the efficiency of perovskite-based optoelectronic devices (solar cells, LEDs and optical amplifiers), without introducing any additional step, and even using different anti-solvent. The method proposed in the present paper offers the possibility to deposit perovskite mixed with many different organic and inorganic compounds, and opens a broad range of applications on perovskite optoelectronic devices as solar cells, LEDs and lasers.

There are several examples of the use of additives for the improvement of perovskite solar cells (PSCs). In most of the cases, these additives are introduced by dissolving them in the solution containing the perovskite precursors,[21] and in other cases a gaseous post treatment after the perovskite film formation is used.[14] When additives are incorporated to

the solution of perovskite precursors, they play an important role in the growth of perovskite film and have an important impact in the film morphology. However, this method is restricted only to additives soluble in the non-polar solution with perovskite precursors.[21] Pyridine vapor exposure of a perovskite film decreases significantly the non-radiative recombination, however this method introduces an additional preparation step.[14] For other perovskite optoelectronic devices, there are significantly lower number of reports on the use of additives. Cho *et al*. reported record LED efficiencies by the use of 2,2′,2″-(1,3,5-benzinetriyl)-tris(1-phenyl-1-H-benzimidazole) (TPBI) additive dissolved in chloroform and using a multistep nanocrystal pinning process.[8b] This deposition process produces nanocrystalline grains, increasing the LED current efficiency. However, this small grain size morphology does not seem to be optimum for solar cells.

We have developed a new approach that takes advantage of the anti-solvent deposition method,[11b, 11c, 18] that is, the method with which the highest PSC record efficiencies have been reported.[11a, 22] In this method, during the spin coating of *N,N*-dimethylformamide (DMF) solution, containing $CH_3NH_3PbI_3$(hereafter $MAPbI_3$) precursors (methylammonium iodide (MAI) and PbI_2), the sample is exposed to a second solvent with a non-polar character in which perovskite precursors are not soluble. This exposure produces the saturation of the solution and the fast precipitation of the precursors creating numerous perovskite nucleation centers and the corresponding formation of a flat, uniform and pinhole-free perovskite layer. Our approach consists of dissolving the additives in the anti-solvent and introduce them in the layer during the anti-solvent step, see the experimental section for more details.

HATNA and DCL97 are not soluble in DMF, which is the common solvent used for PS film fabrication. In this way, to combine PS and the organic compound in a single film, we dispersed the organic additive in an anti-solvent, which was used in the film preparation. Thin films of PS, organic additives and PS with the organic additive using the anti-solvent method have been deposited on glass substrates. The PL spectra of these layers are plotted in Figure

1b and 1c, for samples containing HATNA and DCL97, respectively. The PL spectra of PS and organic single layers are in good agreement with previous reports.[12a, 19a, 20] The PL of perovskite layer containing additives, hereafter PS-HATNA and PS-DCL97, presents PL traces of both compounds, as observed in Figure 1b and 1c, respectively, indicating their presence in the final film after the anti-solvent process. Note that in the case of PS-DCL97, Figure 1c, a new feature at ~650 nm not present in any of the PL spectra of the single layers is observed for the mixed sample. This peak is probably originated in the interaction between both materials, being its interpretation beyond the scope of this manuscript and it is under current research.
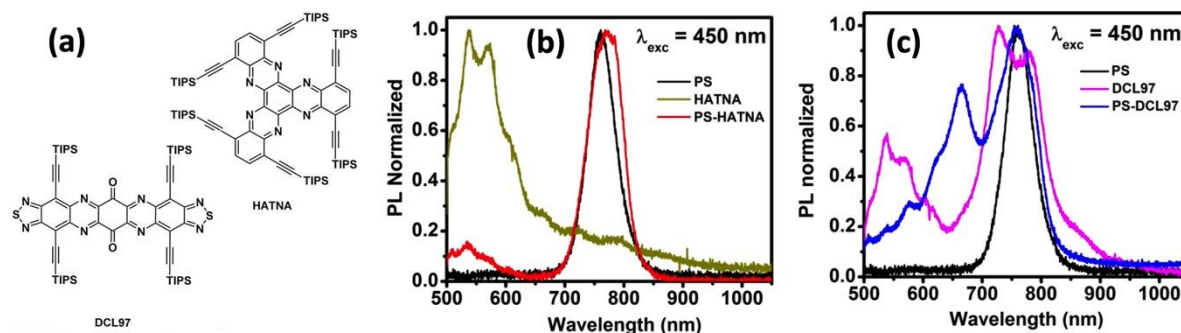
Figure1: a) Scheme of the additives studied in this work. Normalized photoluminescence of perovskite (PS) reference layer **b)** HATNA film and PS with HATNA film and **c)** DCL97 and PS with DCL97.

We have not limited our study to a single type of devices and have extended the study to three different optoelectronic devices: solar cells, LEDs and waveguide optical amplifiers to demonstrate the versatility of this general approach for the optoelectronic field. Solar cells were prepared using compact TiO_2 and spiro-OMeTAD as electron and hole selective contacts, respectively. Two configurations, planar and with TiO_2 mesoporous scaffold, have been analyzed. The current-voltage (J-V) curve for the prepared solar cells showed that the presence of the organic compounds improved the device performance depending on the organic concentration, see Figure S1 and Table S1. The concentration dependence study has been carried out preparing planar PSC samples with the following configuration:

glass/FTO/compact TiO_2 /PS or PS-HATNA or PS- DCL97/spiro-OMeTAD/Au, using

chlorobenzene as anti-solvent. An increase of device efficiency, mainly due to an increase of

the photocurrent, has been detected depending on the concentration, observing the highest

increase for 50 mg/ml and 37.5 mg/ml for HATNA and DCL97(see table S1), respectively. In

addition, solar cells containing mesoporous TiO_2 layer have been prepared with the following

configuration: glass/FTO/compact TiO_2/mesoporousTiO_2 /PS or PS-HATNA or PS-

DCL97/spiro-OMeTAD/Au. For mesoporous configuration HATNA, 50 mg/ml, was

introduced using diethyl ether as the anti-solvent. HATNA presents good solubility on both

diethyl ether and chlorobenzene, but high efficiency reference cells are obtained with diethyl

ether instead of chlorobenzene. DCL97 is not soluble in diethyl ether and consequently

chlorobenzene has been chosen as anti-solvent in that case, allowing us to show the versatility

of the method as it can be employed with different solvents. For TiO_2 mesoporous PSCs, all

the photovoltaic parameters (short circuit current, J_{sc}, open circuit voltage, V_{oc}, fill factor, FF,

and photoconversion efficiency, η) increase for the PS-HATNA sample in comparison with

the reference PS sample, see Figure 2a and Table S2. Concretely, efficiency moves from close

to 12% for the reference sample to close to 15% for PS-HATNA, see Table S2, increasing a

significant ~25%. It is also important to highlight that the PS-HATNA device is practically

hysteresis free, see Figure 2a. In addition, PS-HATNA also presents a better long term

stability behavior, see Figure S2 and Table S2. The analysis of incident photon to current

efficiency (IPCE) shows a good agreement between the integrated photocurrent, see Figure2b,

and the J_{sc} measured in the J-V curve, see Figure2a. In addition, IPCE unveils that the

enhancement in the photocurrent for PS-HATNA samples is not due to the light harvesting

(and subsequent charge collection) from HATNA molecules. IPCE for PS-HATNA has the

same spectra that for the PS reference sample with an increased efficiency in all the

wavelength range, and especially at longer wavelengths where light absorption of HATNA

compound is negligible,[19a] see Figure2b. These results point out to a clear enhancement of

6

the perovskite layer performance by the use of HATNA additive rather than an improvement of the co-absorption by the presence of HATNA. In the case of DCL97, samples with configuration glass/FTO/compact TiO$_2$/mesoporousTiO$_2$ /PS or PS-DCL97/spiro-OMeTAD/Au were also prepared, using chlorobenzene as the anti-solvent. In that case the efficiency of PS-DCL97 has increased ~75% respect a reference cell prepared with chlorobenzene anti-solvent. However in this case the reference samples without DCL97 are far away from optimization presenting a low efficiency, 5%, see Table S3 for more details. Independently of the configuration, molecule employed and anti-solvent, we have observed systematically an increase of efficiency of the prepared solar cells respect the reference samples when additives were used, highlighting the huge potentiality of the method to improve the devices performance. Higher efficiencies can be expected after an accurate optimization process at each concrete configuration.
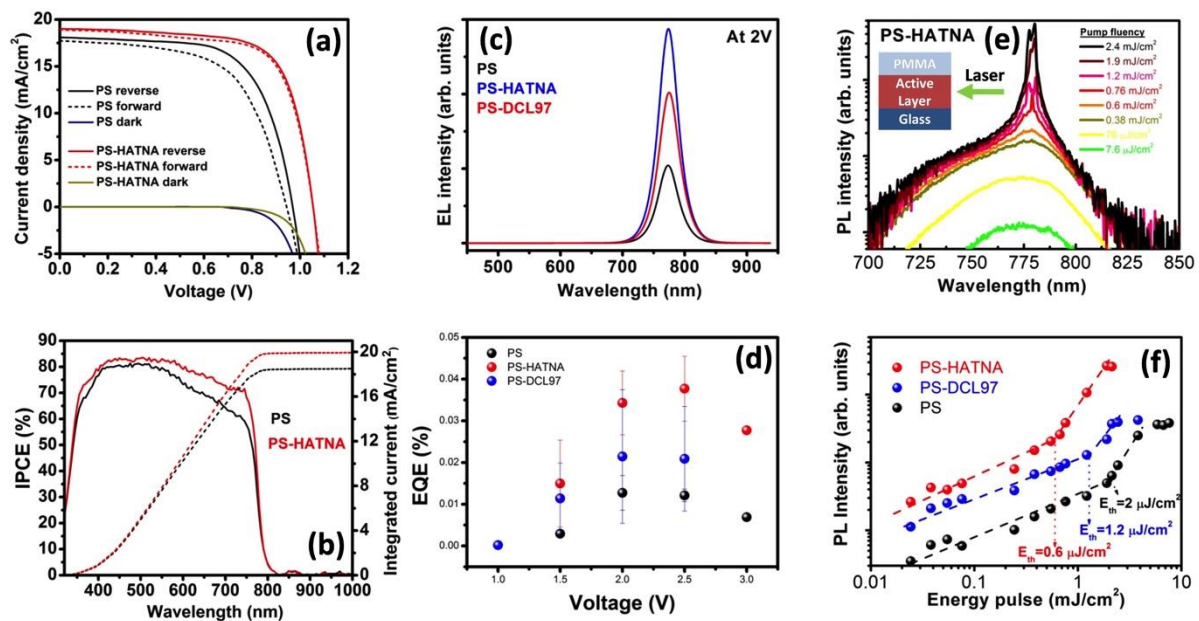
Figure 2: a) Current potential curve of a perovskite reference solar cell and of a perovskite with HATNA additive introduced during the anti-solvent step, under dark and under 1 sun illumination, forward and reverse scans are plotted in order to show the hysteresis behavior. **b)** Incident photon to current efficiency (right axis, solid lines) and the integrated photocurrent (left axis, dashed lines) of the devices depicted in a). **c)** Electroluminescence of

LEDs prepared with perovskite and perovskite with HATNA and DCL97 additives as active layer at an applied forward bias of 2 V. **d)** External quantum efficiency on the prepared LEDs. **e)** Photoluminescence obtained with side excitation,[9] see inset, of perovskite with HATNA additive deposited on glass and with a PMMA capping, see inset. Sample PL has been recorded with different excitation powers. **f)** PL intensity as function of excitation power of perovskite reference and perovskite with HATNA and DCL97 additives films sandwiched between glass and PMMA layers.

MAPbI$_3$ perovskite thin film with organic additives prepared by our method can be applied not only for increasing the performance of light harvesting devices, but also for light emitting systems. LEDs were prepared using PS, PS-HATNA and PS-DCL97 as active layers, and compact TiO$_2$ and spiro-OMeTAD as electron and hole transport materials respectively, following a previously reported configuration.[8a] The electroluminescence (EL) spectra of all the samples (PS, PS-HATNA and PS-DCL97) show only a peak corresponding to the perovskite emission with no parasitic contributions from the organic additives, see Figure 2c. The fabricated LEDs present a remarkably low threshold energy, as low as the MAPbI$_3$ bandgap, see Figure 2d. The use of additives has increased the EQE by a factor of 2 and 4 for DCL97 and HATNA, respectively, as observed in Figure 2d. The EQE presents its maximum value with an applied bias of 2V for the PS and PS-DCL97 samples, while for the PS-HATNA devices the maximum is observed at 2.5 V.

We have also investigated the anti-solvent deposition of additives in perovskite films for light amplification. Waveguide optical amplifier devices were prepared using PS reference layer or PS with organic additives (HATNA or DCL97) as active layer sandwiched between glass and PMMA layer, see inset Figure 2e, following a configuration previously developed by us.[9] These active layers were excited by one of their side faces, see inset Figure 2e, by means of a pulsed laser at 533 nm. Figure 2e shows the emitted light spectra measured at the

opposite face end for the PS-HATNA sample at different pump powers. The spectra for PS and PS-DCL97 planar waveguides are plotted in Figure S3. Waveguided PL spectra correspond to that of the perovskite layer centered around 780 nm, but collapse into a narrow line for high enough pump fluencies (see Figure 2e), which integrated intensity grows superlinearly, as observed in Figure 2f. Both are clear signatures of stimulated emission that exhibits a reduction of the energy threshold by factor of 2 or 4,when the additives DCL97 or HATNA are incorporated respectively into the PS film (Figure 2f and S3). Another characteristic signature of the stimulated emission regime is the decrease of the PL recombination time. Time resolved PL (TRPL) analysis has been carried out to determine the characteristic decay time of the waveguided PL (Figure S4) that reached our experimental system temporal response (and consequently cannot be further determined) for pump fluencies higher than 0.72, 0.5 and 0.1 nJ for PS, PS-DCL97 and PS-HATNA samples, respectively, in good agreement with the lower stimulated emission energy threshold observed in Figure 2f for films made by incorporating additives.

To gain further insight into the origin of the general enhancement in device performance observed for perovskite optoelectronic devices (*i.e.* solar cells, LEDs and optical amplifiers), a systematic characterization by X-Ray Diffraction, scanning electron microscopy (SEM) and impedance spectroscopy (IS) has been carried out. XRD spectra of the films of perovskite with additive do not present any significant variation respect reference perovskite layer produced without additives, see Figure S6, indicating no change in the crystallite size or in the preferential orientation. Moreover, a systematic characterization of the perovskite films prepared with and without additives has been carried out, see Figure S7. The use of additives have a clear interfacial effect. While the use of HATNA produces an organic capping layer, that is removed when spiro-OMeTAD is deposited, the addition of DCL97 changes the roughness and surface morphology, but with no change of perovskite grain size in both cases, see Supporting Information section S7 and Fig. S7 for more details. Consequently a first

9

effect of the additives is the modification of the interface that could induce a beneficial effect in the final cell performance.

PS and PS-HATNA with mesoporous TiO_2 configuration have been analyzed under 0.09 sun intensity at different applied voltages. The obtained Nyquist plots at 0 V are plotted in Figure 3a. Two basic features at high and lower frequencies are observed. The impedance spectra have been fitted using the equivalent circuit recently reported, see Figure S5. Figure 3b plots the resistance of the low frequency arc, R_1, obtained from the fitting of impedance spectra. R_1 is related to the charge carrier recombination (*i.e.* inversely related with the recombination rate).[23] Figure 3b shows the increase in recombination resistance when HATNA additive was introduced into PS film, indicating that the efficiency enhancement observed for devices with additives are due to a decrease of recombination. Dark J-V curves, see Figure 2a, and open circuit voltage decay, see Figure S8, are also in agreement with this conclusion. Impedance spectroscopy cannot determine the origin of the recombination mechanism. However, radiative recombination in perovskite solar cells has been characterized by time-resolved PL, from which we deduce PL decay times in the order of tens-hundreds of ns,[4, 12b] consequently the recombination paths detected by impedance at the µs range and slower scales have a different origin, probably related to non-radiative centers.
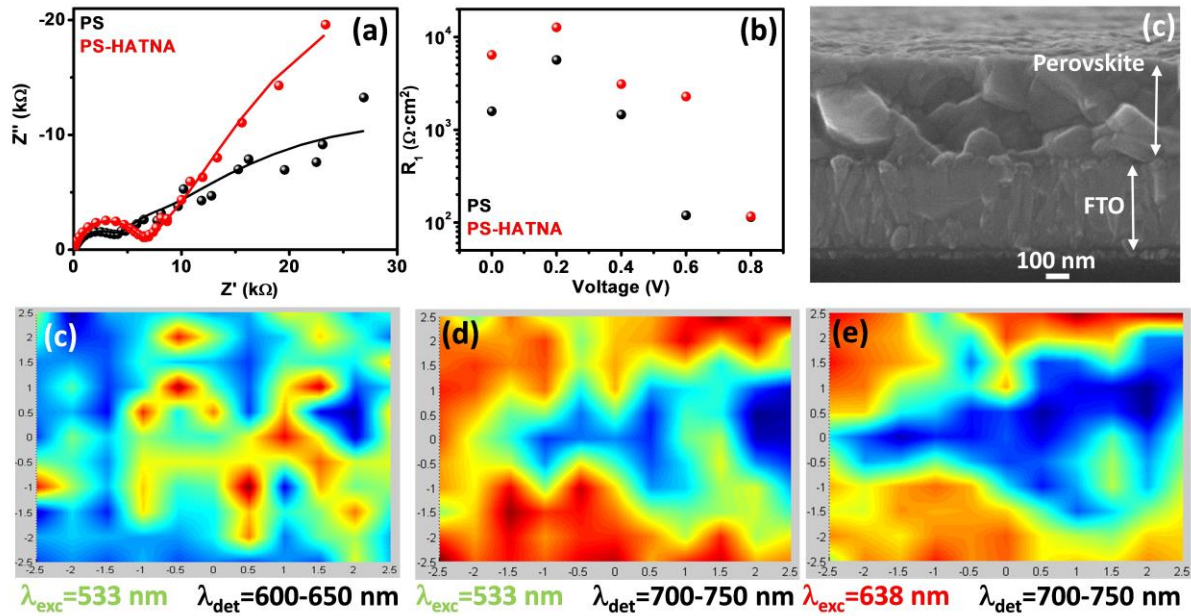
Figure 3: a) Nyquist plot of perovskite and perovskite with HATNA additive solar cells, plotted in Figure 2a,withmesoporous TiO$_2$ configuration and using diethyl ether as anti-solvent, under 0.09 sun illumination at 0 V applied bias. Symbols correspond to the experimental points while solid line is the fitting of the impedance spectra using equivalent circuit in Figure S5.[24] **b)** R$_1$ resistance related with the recombination resistance of perovskite and perovskite with HATNA additive solar cells.[23]**c)** SEM picture of a cross section of perovskite planar layer film. Photoluminescence intensity map of a sample of perovskite with DCL97 additive, excitation wavelength, λ_{exc}, and the range of detected wavelengths, λ_{det}, are indicated in each map. **d)** PL from DCL97, where PL from perovskite has been subtracted, see Figure S9, for further details. **e)** and **f)** PL from perovskite, see Figure S9 for further details, for two different λ_{exc}. Vertical and horizontal scales for the maps are in μm.

Finally, to understand in which way the additives introduced by the anti-solvent deposition method reduces recombination in the perovskite layers beyond the interfacial effect, a PL mapping of the film surface has been carried out using a commercial Scientific Xplora micro-Raman system with 533 nm and 638 nm laser excitation. The integration of PL at

different detection wavelengths, λ_{det}, for PS-DCL97 sample and the subtraction of the PS PL allows to obtain a mapping of the DCL97 PL, Figure 3d, and PS PL, Figure 3e, see Figure S9 for further details of the decoupling of both PL contributions. These results have been doubly checked by using a second excitation wavelength, λ_{exc} =638 nm, see Figure 3f. Comparing, the PL maps in Figures 3d and 3e are clearly complementary: the maximum intensities of PL from DCL97 are observed in areas where the PL from PS is minimum and vice versa. Moreover, the observed PL valleys and peaks form a network with features of hundreds nm size, similar to the grain size observed in PS films by SEM (Figure 3c). A similar analysis performed on different parts of the PS-DCL97 sample surface yielded analogous results, as shown in Figure S10 for the PL map in a different place of the sample surface. This complementary PL emission coinciding with the perovskite grain size points out the hypothesis that DCL97 molecules tend to locate at the grain boundaries of the perovskite film. Hence, the introduction of additives decreases the recombination by the passivation of the grain boundaries. Passivation of grain boundaries has previously shown beneficial effects for the increase of the solar cell photoconversion efficiency,[15] PL emission,[14] and the stability of PS devices.[25]

Through this versatile and general approach (three different optoelectronic devices, two different additive molecules, two different configurations with mesoporous scaffold and planar devices, two different solvents used in the anti-solvent step) we observe a systematic increase of performance in all the devices when additives are used. In this work, we show by XRD that additives do not produce a change in the crystallite size or preferential orientation, while grain size is not modified as it has been determined by the SEM analysis. The main role of additives is the passivation of the grain boundaries and/or perovskite interface for electron-deficient N-PAHs produces a reduction of non-radiative recombination that leads to a notable increase of the main figures of merit of perovskite optoelectronic devices, including solar cells, LEDs and optical amplifiers. The process consists in the introduction of additives in an

anti-solvent during the perovskite spin coating deposition. We have used this method to increase systematically the performance of perovskite solar cells with planar and mesoscopic configurations, the EQE of perovskite LEDs by a factor of 2-4 and to reduce the stimulate emission threshold by a factor of 2-4 by the introduction of DCL97 and HATNA additives in comparison with devices prepared in the same way with the same anti-solvent but without additives. The use of DCL97 and HATNA additives has allowed us to verify the presence of the additives in the prepared film by PL measurements and to track the final situation of these molecules in the film, detecting their presence at the grain boundaries. We have also observed a decrease of the PS recombination due to the use of additives by impedance spectroscopy. These observations point to a passivating effect of the grain boundaries and/or interface by the introduction of additives. It is important to highlight that it is a general method that can be used for the introduction of a broad range of different additives. The design of specific additives with particular properties or functionalizations can enhance further the performance of the optoelectronic devices. For example, the lower threshold energy obtained for the PS-HATNA films in comparison to the PS-DCL97 is probably due to the fact that HATNA does not absorb light at the excitation wavelength, but still passivating the perovskite layer. This work opens an interesting research field on the interaction of perovskite with other compounds with important implications in the enhancement of the perovskite optoelectronic devices.

Experimental Section

*Synthesis of HATNA and DCL97:*The synthesis of HATNA[16i, 19] and DCL97[20] was carried out following previously reported methods and scaled-up accordingly to obtain ~100 mg batches.

TiO$_2$ compact layer: SnO$_2$:F (FTO) substrates were cleaned with soap, sonicated in distilled water, ethanol and a mixture of acetone/isopropanol (30:70 v/v ratio) for 15minutes and then treated with an UV(ultraviolet)−O$_3$lamp for 15minutes. The TiO$_2$ compact layers were

13

manually deposited by spray pyrolysis at 450°C, consuming 5ml of a solution of titanium di-isopropoxidebis (acetylacetonate, 75% vol. 2-propanol) in absolute ethanol (1:9, v/v ratio); the films were annealed at 450°C for 30 minutes.

TiO_2mesoporous (scaffold): TiO_2 paste (Dyesol 30NRd, 30 nm average particle size) dissolved in absolute ethanol (150 mg/ml) was spin coated on TiO_2 compact layers at 1500 rpm from. The films were pre-heated at 100°C for 10 minutes and then at 500°C for 30 minutes.

Perovskite solution: 622 mg (1.35 mmol) of PbI_2 was added in the solution containing 1ml of DMF and 95 μl of dimethyl sulfoxide (DMSO). This solution was heated at 65°C to dissolve PbI_2, then cooled to room temperature. Subsequently PbI_2 solution was poured into a container containing 215 mg (1.35 mmol) of MAI to make final solution for PS deposition.

Perovskite film deposition: PS films were prepared by spin coating at 4000 rpm for substrates with mesoporousTiO_2 scaffolds and at 5000 rpm for substrates only with TiO_2 compact layer. Anti-solvent (chlorobenzene or diethyl ether), ~200 μl, was poured in the films when the spin coater was running after 7 second of the spinning start. Perovskite films were annealed at 65°C for 1 minute and consequently 100°C for 2 minutes.

Organic additive solutions: HATNA and DCL97 solutions were prepared by dissolving HATNA or DCL97 in anti-solvent (diethyl ether and chlorobenzene respectively) separately with the concentration varying from 12.5 to 50 mg/ml. Reference perovskite films have been prepared using both solvents, diethyl ether and chlorobenzene, during the anti-solvent step but without additives. For a fair comparison each sample prepared with additives is compared with a reference perovskite sample which was prepared using the same solvent during the anti-solvent step.

Spiro-OMeTAD and Gold: Spiro-OMeTAD solution was prepared by dissolving 72.3 mg spiro-OMeTAD(2,2′,7,7′-tetrakis(*N,N*-di-*p*-methoxyphenylamine)-9,9-spirobifluorene) in 1 ml of chlorobenzene, then mixed with 28.8 μl of 4-*tert*-butylpyridine and 17.5 μl of a stock

Li$^+$ solution (which contained 520 mg/ml *bis*-trifluoromethylsulfonylamine lithium salt in

acetonitrile). Spiro OMeTAD layer was spin coated on PS or PS with additives films at 4000

rpm for 30s. Finally, 60 nm of gold were thermally evaporated in an ultrahigh vacuum

chamber on top of a Spiro-OMeTAD layer as charge extracting contact.

Characterization: The morphology of the films was analyzed by scanning electron

microscopy (SEM) using a JSM7001F (field emission scanning electron microscope). J-V

curves of solar cells were measured under a xenon arc lamp simulator equipped with an AM

1.5 spectral filter (Sun 2000, ABET Technologies). The intensity was adjusted to provide 1

sun (100 mW cm^{-2}) by using a calibrated silicon solar cell. The *J-V* characteristics were

recorded by scanning the potential from high voltage to zero (reverse mode) and from zero to

high voltage (forward mod) at approximately 45 mV/s.The IPCE measurements were

performed employing a 150 W Xenon lamp coupled with a computer-controlled

monochromator; the photocurrent was measured using an optical power meter 70310 from

Oriel Instruments, using a Si photodiode to calibrate the system. The impedance spectroscopy

measurements were performed under 0.09 sun illumination, calibrated with an NREL-

calibrated Si solar cell, and under N_2 flow. The measurements were carried out by means of a

FRA equipped PGSTAT-30 from Autolab at different forward voltage bias and applying a 20

mV voltage AC perturbation over the constant applied bias with the frequency ranging

between 1 MHz and 0.05 Hz. The use of 0.09 sun illumination prevent cell degradation during

the impedance measurement, see Fig. S11, and also keep the illumination conditions as it has

been shown that working conditions of perovskite layer varies significantly when the layer is

illuminated.[23b] The EL spectra of LED devices based on PS absorber without and with

organic compounds (HATNA or DCL97) in situ were obtained by using a spectrophotometer

based on a CCD detector (Andor-iDUSDV420A-OE) synchronized with the potentiostat

(Gamry Reference 3000). The combination of both apparatus allowed registering optical

variations (absorbance, transmittance, light emission, etc.) while applying an external

electrical stimulus (voltage or current) with a maximum time resolution in the milliseconds

scale. EL measurements have been carried out under dark conditions and under N_2 flow at

room temperature. The EQE measurements were performed by calibrating the optical

equipment with a commercial GaAs infrared LED (model EL-23G, peak emission centered at

λ_{max}= 940 nm, 28.3 W·sr^{-1}·m^{-2}). Photoluminescence (PL)experiments were carried out by

pumping the surface of the samples with a 533 nm DSPP (diode pumped solid state) laser and

a 780 nm semiconductor diode. Back scattered PL was then collected with the aid of a

microscope objective and dispersed in an Ocean Optics HR4800 spectrograph.

Stimulated emission experiments were performed by exciting the surface of the samples with

aNd:Yag533nm pulsed laser (1 ns 20 KHz) and collecting the emitted PL with a 20x

microscope objective. PL spectra were obtained by dispersing the light in an Ocean Optics

HR4800 spectrograph, and time resolved photoluminescence (TRPL) were carried out by

focusing the PL into a Hamamatsu C5658-3769 avalanche photodetector connected to a

BOXCARDPCS-150 electronics from Becker &Hickl GmbH. The PL map were obtained by

using a commercial Scientific Xplora micro-Raman system with 533 nm and 638 nm laser

excitation. XRD has been characterized employing a Bruker AXS-D4 Endeaver Advance X-

ray diffractometer using Cu Ka radiation.

Supporting Information
Supporting Information is available online from the Wiley Online Library or from the author.

Received: ((will be filled in by the editorial staff))
Revised: ((will be filled in by the editorial staff))
Published online: ((will be filled in by the editorial staff))

[1]   a) T. M. Brenner, D. A. Egger, L. Kronik, G. Hodes, D. Cahen, *Nature Reviews Materials* **2016**, *1*, 15007;b) M. A. Green, A. Ho-Baillie, H. J. Snaith, *Nat Photon* **2014**, *8*, 506-514;c) S. D. Stranks, H. J. Snaith, *Nat Nano* **2015**, *10*, 391-402;d) B. R. Sutherland, E. H. Sargent, *Nat Photon* **2016**, *10*, 295-302.

[2]   S. De Wolf, J. Holovsky, S.-J. Moon, P. Löper, B. Niesen, M. Ledinsky, F.-J. Haug, J.-H. Yum, C. Ballif, *The Journal of Physical Chemistry Letters* **2014**, *5*, 1035-1039.

[3]   a) W.-J. Yin, T. Shi, Y. Yan, *Advanced Materials* **2014**, *26*, 4653-4658;b) W.-J. Yin, T. Shi, Y. Yan, *Applied Physics Letters* **2014**, *104*, 063903.

[4]   a) S. D. Stranks, G. E. Eperon, G. Grancini, C. Menelaou, M. J. P. Alcocer, T. Leijtens, L. M. Herz, A. Petrozza, H. J. Snaith, *Science* **2013**, *342*, 341-344;b) G. Xing, N. Mathews, S. Sun, S. S. Lim, Y. M. Lam, M. Grätzel, S. Mhaisalkar, T. C. Sum, *Science* **2013**, *342*, 344-347.

[5]   a) W. Tress, N. Marinova, O. Inganäs, M. K. Nazeeruddin, S. M. Zakeeruddin, M. Graetzel, *Advanced Energy Materials* **2015**, *5*, n/a-n/a;b) J. S. Manser, P. V. Kamat, *Nat Photon* **2014**, *8*, 737-743;c) D. Bi, W. Tress, M. I. Dar, P. Gao, J. Luo, C. Renevier, K. Schenk, A. Abate, F. Giordano, J.-P. Correa Baena, J.-D. Decoppet, S. M. Zakeeruddin, M. K. Nazeeruddin, M. Grätzel, A. Hagfeldt, *Science Advances* **2016**, *2*, e1501170.

[6]   M. A. Green, K. Emery, Y. Hishikawa, W. Warta, E. D. Dunlop, *Progress in Photovoltaics: Research and Applications* **2016**, *24*, 905-913.

[7]   A. Kojima, K. Teshima, Y. Shirai, T. Miyasaka, *Journal of the American Chemical Society* **2009**, *131*, 6050-6051.

[8]   a) O. A. Jaramillo-Quintero, R. S. Sanchez, M. Rincon, I. Mora-Sero, *The Journal of Physical Chemistry Letters* **2015**, *6*, 1883-1890;b) H. Cho, S.-H. Jeong, M.-H. Park, Y.-H. Kim, C. Wolf, C.-L. Lee, J. H. Heo, A. Sadhanala, N. Myoung, S. Yoo, S. H. Im, R. H. Friend, T.-W. Lee, *Science* **2015**, *350*, 1222-1225;c) Z.-K. Tan, R. S. Moghaddam, M. L. Lai, P. Docampo, R. Higler, F. Deschler, M. Price, A. Sadhanala, L. M. Pazos, D. Credgington, F. Hanusch, T. Bein, H. J. Snaith, R. H. Friend, *Nat Nano* **2014**, *9*, 687-692;d) L. Gil-Escrig, G. Longo, A. Pertegas, C. Roldan-Carmona, A. Soriano, M. Sessolo, H. J. Bolink, *Chemical Communications* **2015**, *51*, 569-571;e) Y.-H. Kim, H. Cho, J. H. Heo, T.-S. Kim, N. Myoung, C.-L. Lee, S. H. Im, T.-W. Lee, *Advanced Materials* **2015**, *27*, 1248-1254.

[9]   I. Suárez, E. J. Juárez-Pérez, J. Bisquert, I. Mora-Seró, J. P. Martínez-Pastor, *Advanced Materials* **2015**, *27*, 6157-6162.

[10]   a) G. Xing, N. Mathews, S. S. Lim, N. Yantara, X. Liu, D. Sabba, M. Grätzel, S. Mhaisalkar, T. C. Sum, *Nat Mater* **2014**, *13*, 476-480;b) F. Deschler, M. Price, S.

Pathak, L. E. Klintberg, D.-D. Jarausch, R. Higler, S. Hüttner, T. Leijtens, S. D. Stranks, H. J. Snaith, M. Atatüre, R. T. Phillips, R. H. Friend, *The Journal of Physical Chemistry Letters* **2014**, *5*, 1421-1426;c) H. Zhu, Y. Fu, F. Meng, X. Wu, Z. Gong, Q. Ding, M. V. Gustafsson, M. T. Trinh, S. Jin, X. Y. Zhu, *Nat Mater* **2015**, *14*, 636-642.

[11]   a) W. S. Yang, J. H. Noh, N. J. Jeon, Y. C. Kim, S. Ryu, J. Seo, S. I. Seok, *Science* **2015**, *348*, 1234-1237;b) N. J. Jeon, J. H. Noh, Y. C. Kim, W. S. Yang, S. Ryu, S. I. Seok, *Nat Mater* **2014**, *13*, 897-903;c) N. Ahn, D.-Y. Son, I.-H. Jang, S. M. Kang, M. Choi, N.-G. Park, *Journal of the American Chemical Society* **2015**, *137*, 8696-8699.

[12]   a) T. T. Ngo, I. Suarez, R. S. Sanchez, J. P. Martinez-Pastor, I. Mora-Sero, *Nanoscale* **2016**;b) R. S. Sanchez, M. S. de la Fuente, I. Suarez, G. Muñoz-Matutano, J. P. Martinez-Pastor, I. Mora-Sero, *Science Advances* **2016**, *2*, e1501104;c) X. Gong, Z. Yang, G. Walters, R. Comin, Z. Ning, E. Beauregard, V. Adinolfi, O. Voznyy, E. H. Sargent, *Nat Photon* **2016**, *10*, 253-257;d) Z. Ning, X. Gong, R. Comin, G. Walters, F. Fan, O. Voznyy, E. Yassitepe, A. Buin, S. Hoogland, E. H. Sargent, *Nature* **2015**, *523*, 324-328;e) S.-S. Li, C.-H. Chang, Y.-C. Wang, C.-W. Lin, D.-Y. Wang, J.-C. Lin, C.-C. Chen, H.-S. Sheu, H.-C. Chia, W.-R. Wu, U. S. Jeng, C.-T. Liang, R. Sankar, F.-C. Chou, C.-W. Chen, *Energy & Environmental Science* **2016**, *9*, 1282-1289.

[13]   S. F. Völker, S. Collavini, J. L. Delgado, *ChemSusChem* **2015**, *8*, 3012-3028.

[14]   D. W. de Quilettes, S. M. Vorpahl, S. D. Stranks, H. Nagaoka, G. E. Eperon, M. E. Ziffer, H. J. Snaith, D. S. Ginger, *Science* **2015**, *348*, 683-686.

[15]   Y. Shao, Z. Xiao, C. Bi, Y. Yuan, J. Huang, *Nat Commun* **2014**, *5*, 5784.

[16]   a) A. Mateo-Alonso, *Chem. Soc. Rev.* **2014**, *43*, 6311--6324;b) U. H. F. Bunz, J. U. Engelhart, B. D. Lindner, M. Schaffroth, *Angew. Chem. Int. Ed.* **2013**, *52*, 3810-3821;c) U. H. F. Bunz, *Chem. Eur. J.* **2009**, *15*, 6780-6789;d) M. Stępień, E. Gońka, M. Żyła, N. Sprutta, *Chem. Rev.* **2016**;e) A. B. Marco, C. Gozalvez, M. Olano, X. Sun, A. Atxabal, M. Melle-Franco, L. E. Hueso, A. Mateo-Alonso, *Physical Chemistry Chemical Physics* **2016**, *18*, 11616-11619;f) L. Jiang, A. C. Papageorgiou, S. C. Oh, Ö. Sağlam, J. Reichert, D. A. Duncan, Y.-Q. Zhang, F. Klappenberger, Y. Guo, F. Allegretti, S. More, R. Bhosale, A. Mateo-Alonso, J. V. Barth, *ACS Nano* **2016**, *10*, 1033-1041;g) A. B. Marco, D. Cortizo-Lacalle, C. Gozalvez, M. Olano, A. Atxabal, X. Sun, M. Melle-Franco, L. E. Hueso, A. Mateo-Alonso, *Chem. Commun.* **2015**, *51*, 10754-10757;h) R. Garcia, M. Melle-Franco, A. Mateo-Alonso, *Chem. Commun.* **2015**, *51*, 8037-8040;i) D. Cortizo-Lacalle, A. Pertegas, L. Martinez-Sarti, M. Melle-Franco, H. J. Bolink, A. Mateo-Alonso, *J. Mater. Chem. C* **2015**, *3*, 9170-9174;j) S. More, S. Choudhary, A. Higelin, I. Krossing, M. Melle-Franco, A. Mateo-Alonso, *Chem. Commun.* **2014**, *50*, 1976-1979;k) S. More, R. Bhosale, A. Mateo-Alonso, *Chem. Eur. J.* **2014**, *20*, 10626–10631;l) M. Grzelczak, N. Kulisic, M. Prato, A. Mateo-Alonso, *Part. Part. Syst. Charact.* **2014**, *31*, 121-125;m) R. García, S. More, M. Melle-Franco, A. Mateo-Alonso, *Org. Lett.* **2014**, *16*, 6096-6099;n) S. More, R. Bhosale, S. Choudhary, A. Mateo-Alonso, *Org. Lett.* **2012**, *14*, 4170-4173;o) N. Kulisic, S. More, A. Mateo-Alonso, *Chem. Commun.* **2011**, *47*, 514-516;p) A. Mateo-Alonso, N. Kulisic, G. Valenti, M. Marcaccio, F. Paolucci, M. Prato, *Chem. Asian. J.* **2010**, *5*, 482-485;q) M. Grzelczak, N. Kulisic, M. Prato, A. Mateo-Alonso, *Chem. Commun.* **2010**, *46*, 9122-9124;r) A. Mateo-Alonso, C. Ehli, K. H. Chen, D. M. Guldi, M. Prato, *J. Phys. Chem. A* **2007**, *111*, 12669-12673;s) A. M. Alonso, R. Horcajada, M. Motevalli, J. H. P. Utley, P. B. Wyatt, *Org. Biomol. Chem.* **2005**, *3*, 2842-2847;t) A. M. Alonso, R. Horcajada, H. J. Groombridge, R. Chudasama, M. Motevalli, J. H. P. Utley, P. B. Wyatt, *Org. Biomol. Chem.* **2005**, *3*, 2832-2841;u) A. M. Alonso, R. Horcajada, H. J. Groombridge, R. Mandalia, M. Motevalli, J. H. P. Utley, P. B. Wyatt, *Chem. Commun.* **2004**, 412-413;v) G. J. Richards, J. P. Hill, T. Mori, K. Ariga, *Org. Biomol. Chem.* **2011**, *9*, 5005-5017;w) U. H. F. Bunz, *Pure and Applied Chemistry*

2010, *82*, 953-968;x) G. J. Richards, J. P. Hill, N. K. Subbaiyan, F. D'Souza, P. A. Karr, M. R. J. Elsegood, S. J. Teat, T. Mori, K. Ariga, *J. Org. Chem.* **2009**, *74*, 8914-8923.

[17]   a) J. E. Anthony, A. Facchetti, M. Heeney, S. R. Marder, X. Zhan, *Adv. Mater.* **2010**, *22*, 3876-3892;b) Z. Liang, Q. Tang, J. Liu, J. Li, F. Yan, Q. Miao, *Chemistry of Materials* **2010**, *22*, 6438-6443.

[18]   M. Xiao, F. Huang, W. Huang, Y. Dkhissi, Y. Zhu, J. Etheridge, A. Gray-Weale, U. Bach, Y.-B. Cheng, L. Spiccia, *Angewandte Chemie* **2014**, *126*, 10056-10061.

[19]   a) G. Tregnago, C. Fléchon, S. Choudhary, C. Gozalvez, A. Mateo-Alonso, F. Cacialli, *App. Phys. Lett.* **2014**, *105*, 143304;b) F. Selzer, C. Falkenberg, M. Hamburger, M. Baumgarten, K. Müllen, K. Leo, M. Riede, *Journal of Applied Physics* **2014**, *115*, 054515;c) J. Clark, R. Archer, T. Redding, C. Foden, J. Tant, Y. Geerts, R. H. Friend, C. Silva, *J. App. Phys.* **2008**, *103*, 124510.

[20]   D. Cortizo-Lacalle, C. Gozalvez, M. Olano, X. Sun, M. Melle-Franco, L. E. Hueso, A. Mateo-Alonso, *Organic Letters* **2015**, *17*, 5902-5905.

[21]   a) X. Li, M. Ibrahim Dar, C. Yi, J. Luo, M. Tschumi, S. M. Zakeeruddin, M. K. Nazeeruddin, H. Han, M. Grätzel, *Nat Chem* **2015**, *7*, 703-711;b) P.-W. Liang, C.-Y. Liao, C.-C. Chueh, F. Zuo, S. T. Williams, X.-K. Xin, J. Lin, A. K. Y. Jen, *Advanced Materials* **2014**, *26*, 3748-3754;c) C.-Y. Chang, C.-Y. Chu, Y.-C. Huang, C.-W. Huang, S.-Y. Chang, C.-A. Chen, C.-Y. Chao, W.-F. Su, *ACS Applied Materials & Interfaces* **2015**, *7*, 4955-4961;d) Q. Dong, Z. Wang, K. Zhang, H. Yu, P. Huang, X. Liu, Y. Zhou, N. Chen, B. Song, *Nanoscale* **2016**, *8*, 5552-5558;e) C.-C. Chueh, C.-Y. Liao, F. Zuo, S. T. Williams, P.-W. Liang, A. K. Y. Jen, *Journal of Materials Chemistry A* **2015**, *3*, 9058-9062.

[22]   M. Saliba, T. Matsui, J.-Y. Seo, K. Domanski, J.-P. Correa-Baena, M. K. Nazeeruddin, S. M. Zakeeruddin, W. Tress, A. Abate, A. Hagfeldt, M. Gratzel, *Energy & Environmental Science* **2016**, *9*, 1989-1997.

[23]   a) A. Dualeh, T. Moehl, N. Tétreault, J. Teuscher, P. Gao, M. K. Nazeeruddin, M. Grätzel, *ACS Nano* **2014**, *8*, 362-373;b) E. J. Juarez-Perez, R. S. Sanchez, L. Badia, G. Garcia-Belmonte, Y. S. Kang, I. Mora-Sero, J. Bisquert, *The Journal of Physical Chemistry Letters* **2014**, *5*, 2390-2394;c) V. Gonzalez-Pedro, E. J. Juarez-Perez, W.-S. Arsyad, E. M. Barea, F. Fabregat-Santiago, I. Mora-Sero, J. Bisquert, *Nano Letters* **2014**, *14*, 888-893;d) B. Suarez, V. Gonzalez-Pedro, T. S. Ripolles, R. S. Sanchez, L. Otero, I. Mora-Sero, *The Journal of Physical Chemistry Letters* **2014**, *5*, 1628-1635.

[24]   A. Guerrero, G. Garcia-Belmonte, I. Mora-Sero, J. Bisquert, Y. S. Kang, T. J. Jacobsson, J.-P. Correa-Baena, A. Hagfeldt, *The Journal of Physical Chemistry C* **2016**, *120*, 8023-8032.

[25]   T. A. Berhe, W.-N. Su, C.-H. Chen, C.-J. Pan, J.-H. Cheng, H.-M. Chen, M.-C. Tsai, L.-Y. Chen, A. A. Dubale, B.-J. Hwang, *Energy & Environmental Science* **2016**, *9*, 323-356.

[26]   I. Zarazua, J. Bisquert, G. Garcia-Belmonte, *The Journal of Physical Chemistry Letters* **2016**, *7*, 525-528.

The table of contents

We report a novel method in order to increase the efficiency of perovskite optoelectronic devices demonstration its goodness for perovskite solar cells, LEDs and optical amplifiers. The method is based on the introduction of organic additives during the anti-solvent step in the perovskite thin film deposition process. Additives passivate grain boundaries reducing the non-radiative recombination. The method can be easily extended to other additives.

Keyword perovskite, solar cell, LED, optical amplifier, recombination

Thi Tuyen Ngo, Isaac Suarez, Gabriella Antonicelli, Diego Cortizo-Lacalle, Juan P. Martinez-Pastor,* Aurelio Mateo-Alonso* and Ivan Mora-Sero*

Title Enhancement of the Performance of Perovskite Solar Cells, LEDs and Optical Amplifiers by Anti-Solvent Additive Deposition

ToC figure
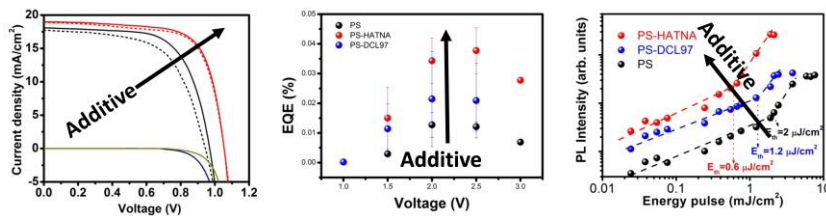
Supporting Information

Enhancement of the Performance of Perovskite Solar Cells, LEDs and Optical Amplifiers by Anti-Solvent Additive Deposition

Thi Tuyen Ngo, Isaac Suarez, Gabriella Antonicelli, Diego Cortizo-Lacalle, Juan P. Martinez-Pastor,* Aurelio Mateo-Alonso* and Ivan Mora-Sero*

S1. Study of the solar cell performance as function the additive concentration.
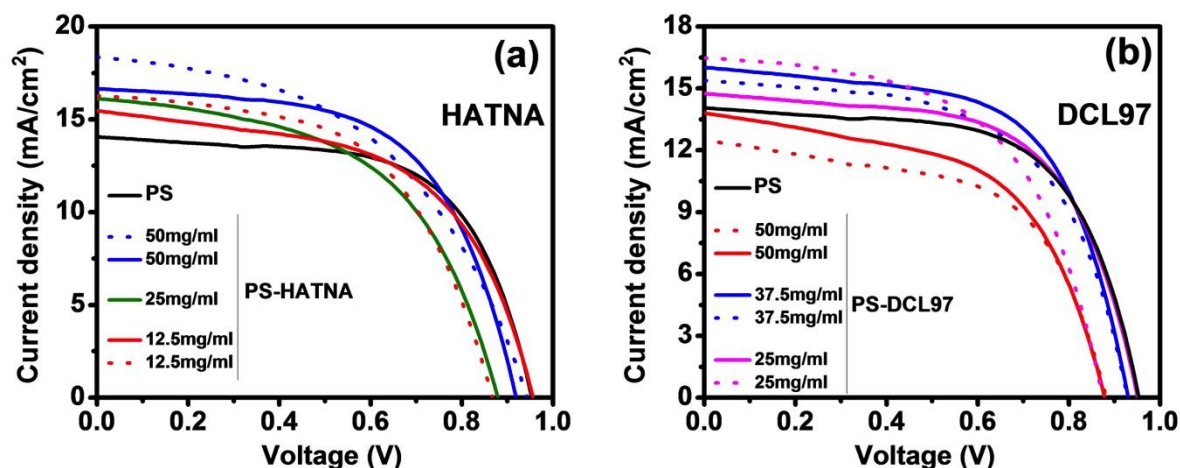
Figure S1. J-V curves solar cells with planar configuration (no-mesoporous TiO_2 layer) using

(**a**) PS-HATNA and (**b**) PS-DCL97 films as light harvesting layers in a comparison with

reference PS samples, without organic additive. Active PS, PS-HATNA and PS-DCL97

layers were spin coated on TiO_2 compact at 5000 rpm, annealed at 65^oC for 1 minute and

100^oC for 2 minutes consequently. PS-organic film was prepared using a solution of organic

compounds dispersed in chlorobenzene with different concentration from 12.5 to 50 mg/ml as

an anti-solvent.

Table S1: Average photovoltaic parameters (short circuit current, J_{sc}, open circuit voltage, V_{oc}, fill factor, FF, and photoconversion efficiency, η) under AM1.5 simulated sunlight for planar perovskite solar cell configuration (glass/FTO/compact TiO_2 /PS or PS-HATNA or PS-DCL97/spiro-OMeTAD/Au). At least five cells have been prepared at each condition.

Organic	Concentration Mg/ml	Jsc (mA/cm^2)	Voc (V)	FF (%)	η %
No (Ref)	0	13.4 ± 0.3	0.89 ± 0.01	57.0 ± 1.0	6.9 ± 0.3
HATNA	50	16.8 ± 0.4	0.94 ± 0.01	53.0 ± 2.0	8.42 ± 0.24
HATNA	25	14.2 ± 1.1	0.89 ± 0.14	49.0 ± 4.0	6.3 ± 0.9
HATNA	12.5	15.7 ± 0.5	0.88 ± 0.02	52.3 ± 2.0	7.07 ± 0.52
DCL97	50	11.9 ± 0.5	0.88 ± 0.01	56.1 ± 0.7	5.8 ± 0.3
DCL97	37.5	14.9 ± 0.4	0.920 ± 0.003	59.1 ± 0.8	8.1 ± 0.30
DCL97	25	14.3 ± 0.6	0.90 ± 0.02	57.5 ± 0.8	7.39 ± 0.4

S2. Study of the stability of solar cell performance.
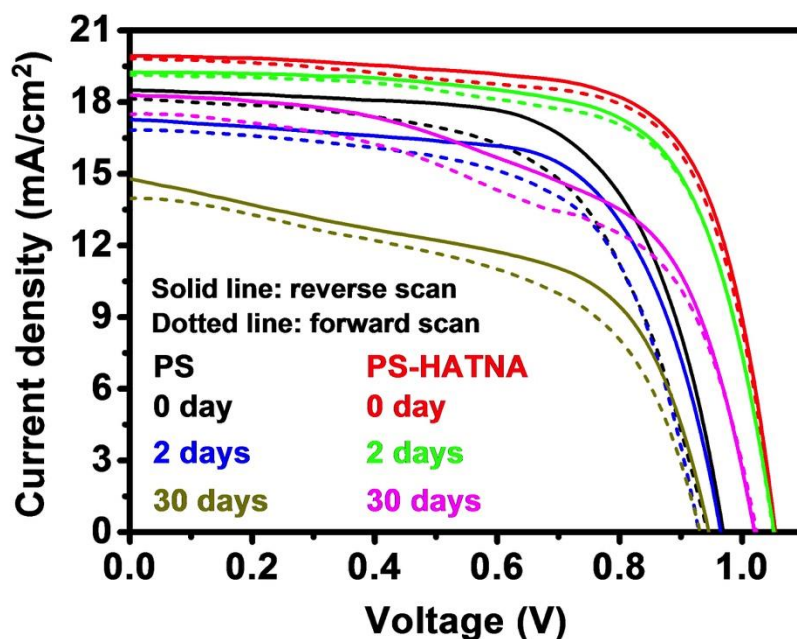
Figure S2. J-V curves solar cells with mesoporous configuration using PS without (reference) and with HATNA additive, at different times after solar cell preparation. In which absorber layers were spin coated on mesoporousTiO$_2$ at 4000 rpm, annealed at 65°C for 1 minute and 100°C for 2 minutes consequently. PS-HATNA film was prepared using a solution of HATNA compounds dispersed in diethyl ether with the concentration of 50 mg/ml. Solar cell were stored on ambient conditions under dark.

Table S2: Photovoltaic parameters(short circuit current, J_{sc}, open circuit voltage, V_{oc}, fill factor, FF, and photoconversion efficiency, η), at different times after solar cell preparation, under AM1.5 simulated sunlight for mesoporous perovskite solar cell configuration (glass/FTO/compact TiO_2/mesoporousTiO_2/PS or PS-HATNA/spiro-OMeTAD/Au).Solar cell were stored on ambient conditions under dark. rev: reverse J-V scan; for: forward J-V scan

Samples	0 day				2 days				30 days			
	PS		PS-HATNA		PS		PS-HATNA		PS		PS-HATNA	
	rev	for	rev	for	rev	for	rev	for	rev	for	rev	for
Jsc (mA/cm^2)	18.50	18.15	19.93	19.82	17.27	16.87	19.26	19.16	14.78	13.66	18.31	17.54
Voc (V)	0.969	0.943	1.054	1.054	0.964	0.929	1.052	1.051	0.945	0.931	1.02	1.023
FF (%)	65.6	60.5	70.8	70	65.6	63.1	69.2	68.8	56.2	55.1	57.9	55.8
η (%)	11.76	10.35	14.87	14.62	10.92	9.89	14.02	13.85	7.85	7.01	10.81	10.01

Table S3: Avarage photovoltaic parameters (short circuit current, J_{sc}, open circuit voltage, V_{oc}, fill factor, FF, and photoconversion efficiency, η) under AM1.5 simulated sunlight for mesoporous perovskite solar cell configuration (glass/FTO/$TiO_{2\_compact}$ /TiO_{2_meso}/PS or PS-DCL97/spiro-OMeTAD/Au) in which DCL97 was dispersed in chlorobenzene with the concentration of 37.5 mg/ml

	Jsc (mA/cm^2)	Voc (V)	FF (%)	η (%)
PS	9.2 ± 0.4	0.870 ± 0.007	63.0 ± 2.0	5.0 ± 0.3
PS-DCL97	13.7 ± 0.6	0.891 ± 0.014	72.2 ± 1.2	8.9 ± 0.5

S3. Photoluminescence at different excitation power for waveguide light amplifying devices.
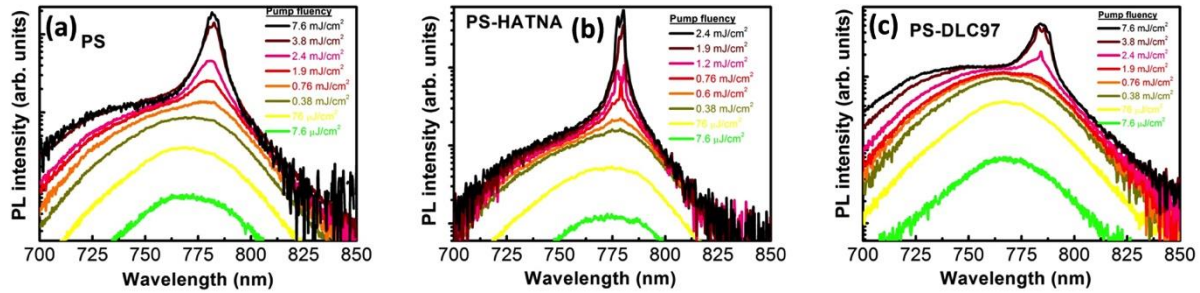
Figure S3. Photoluminescence obtained with side excitation,[9] see inset Figure 2e, of **(a)** reference PS; **(b)** PS-HATNAand **(c)** PS-DCL97 additive deposited on glass and with a PMMA capping, see inset Figure 2e. Sample PL has been recorded with different excitation powers.

S4. Time Resolved Photoluminescence for waveguide light amplifying devices.

Time Resolved Photoluminescence (TRPL) measurements were fitted with the following equation in order to extract the recombination times involved in the system:

$$I = A \cdot \left(e^{-\frac{t}{\tau_1}} - e^{-\frac{t}{\tau_{rise}}} \right) + B \cdot e^{-\frac{t}{\tau_2}} + C \cdot e^{-\frac{t}{\tau_3}} \tag{1}$$

Here τ_{rise} was fixed to 10 ps and $\tau_1, \tau_2 \tau_3$, A, B, C are fitting parameters.

TRPL for PS reference sample, see Figure S4a, can be fitted with two exponential decays. The long one is about 5 ns, and the shorts starts from 0.4-0.5 ns to 0.02-0.1 ns (response of the system). For high powers, it becomes necessary to include a third exponential decay with a small width to improve the fitting a bit. Curve presented the same spectra (response of the system reached) for pump fluencies higher than 0.72 nJ. When additives are added to the PS film, Figure S4b and S4c, it becomes necessary to include a third exponential decay, even for low excitation fluencies. Indeed, recombination times do not change (τ_1=20-100ps, τ_2=400-500 ps, τ_3=5ns) with the excitation, but only the weights (A,B,C). The higher the excitation fluency, the weight A (shorter time) becomes more and more important. Curves

25

presented the same spectra (response of the system reached) for pump fluencies higher than

0.1 nJ and 0.5 nJ for HATNA and DCL97, respectively.
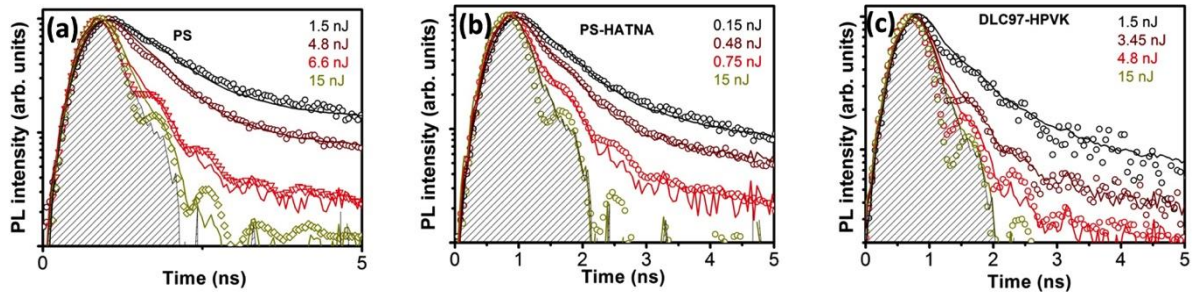
Figure S4. Time Resolved Photoluminescence (TRPL) for waveguide light amplifying

devices with an active layer of **(a)** reference PS; **(b)** PS-HATNAand **(c)** PS-DCL97 additive,

deposited on glass and with a PMMA capping, see inset Figure 2e. TRPL has been recorded

with different excitation powers. Shadow area represents the response of the system.

S5. Equivalent circuit using for fitting the impedance results.
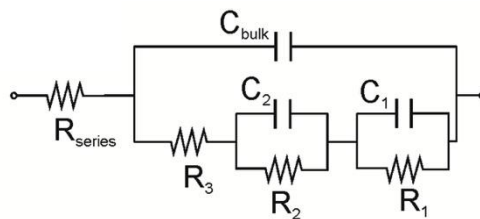
Figure S5. Equivalent circuit for PSCs.[24] R_{series} is the series resistance of substrate and

wiring, C_{bulk} is the geometrical capacitance of the sample. R_2 and C_2 are resistance and

capacitance related with the contact/perovskite interface, C_1 has been related with an

accumulation capacitance[26] while R_1 is related with the recombination resistance (inversely

related with the recombination rate).[23]

S6. X-Ray Diffraction (XRD).
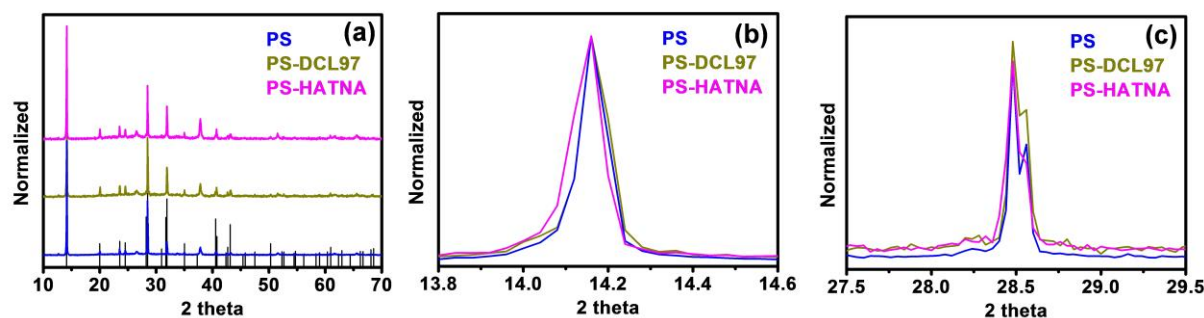
Figure S6. **(a)** Normalized intensity of XRD spectra, black lines correspond to powder pattern of MAPbI$_3$. **(b)** Zoom of the peak for diffractions corresponding to (110) and (002) planes. **(c)** Zoom of the peak for diffractions corresponding to (220) and (004) planes.

S7. Scanning Electron Microscopy (SEM).

SEM analysis permits to highlight differences between the two additives. While HATNA solved in diethyl ether produces a layer on top of the perovskite film see Fig. S7l and m, this is not the case of DCL97 solved in chlorobenzene, where no capping layer on top of perovskite was observed, see Fig. S7 c and d. The HATNA layer is removed during the deposition of spiro-OMeTAD solved in chlorobenzene as HATNA is soluble in this solvent, see Fig. S7p and q. Moreover, addition of DCL97 produces a change of the surface roughness, as it can be clearly appreciated from the comparison between Fig. S7e and Fig. S7f which are the top views of PS layer without and with DCL97 additive, respectively, using chlorobenzene as anti-solvent. This observation points to a change in the interfacial properties of layer with additives that could have a beneficial effect in the performance of the optoelectronic devices. While in perovskite layer without DCL97 additive the grains of perovskite are clearly recognized, see Fig. S7e, when DCL97 is added during the anti-solvent step the surface morphology changes making difficult to observe the grains, see Fig. S7f. However from cross section, see Fig. S7a and c, it can be observed that no significant change in the grain size is produced when DCL97 is added.

27

In the case of HATNA, added using diethyl ether as anti-solvent, a clear different behavior is observed with the formation of a HATNA capping layer on top of the perovskite layer, see Fig. S7l and S7m, and top view Fig. S7h. Nevertheless, as in the case of DCL97, no significant change in grain size has been detected, compare Fig. S7i and S7l. It is important to highlight that HATNA capping is removed when spiro-OMeTAD is deposited as HATNA is soluble in chlorobenzene where spiro-OMeTAD is solved, resulting in a similar thickness for organic capping layers observed in full devices without and with HATNA additives corresponding to the spiro-OMeTAD film, see Fig. S7o and S7q.

Finally, note that reference samples present larger grain size when diethyl ether is used as anti-solvent instead of chlorobenzene, compare Fig. S7g and S7e, producing a lower performance for samples fabricated with chlorobenzene, compare Fig. 2a and Table S3.
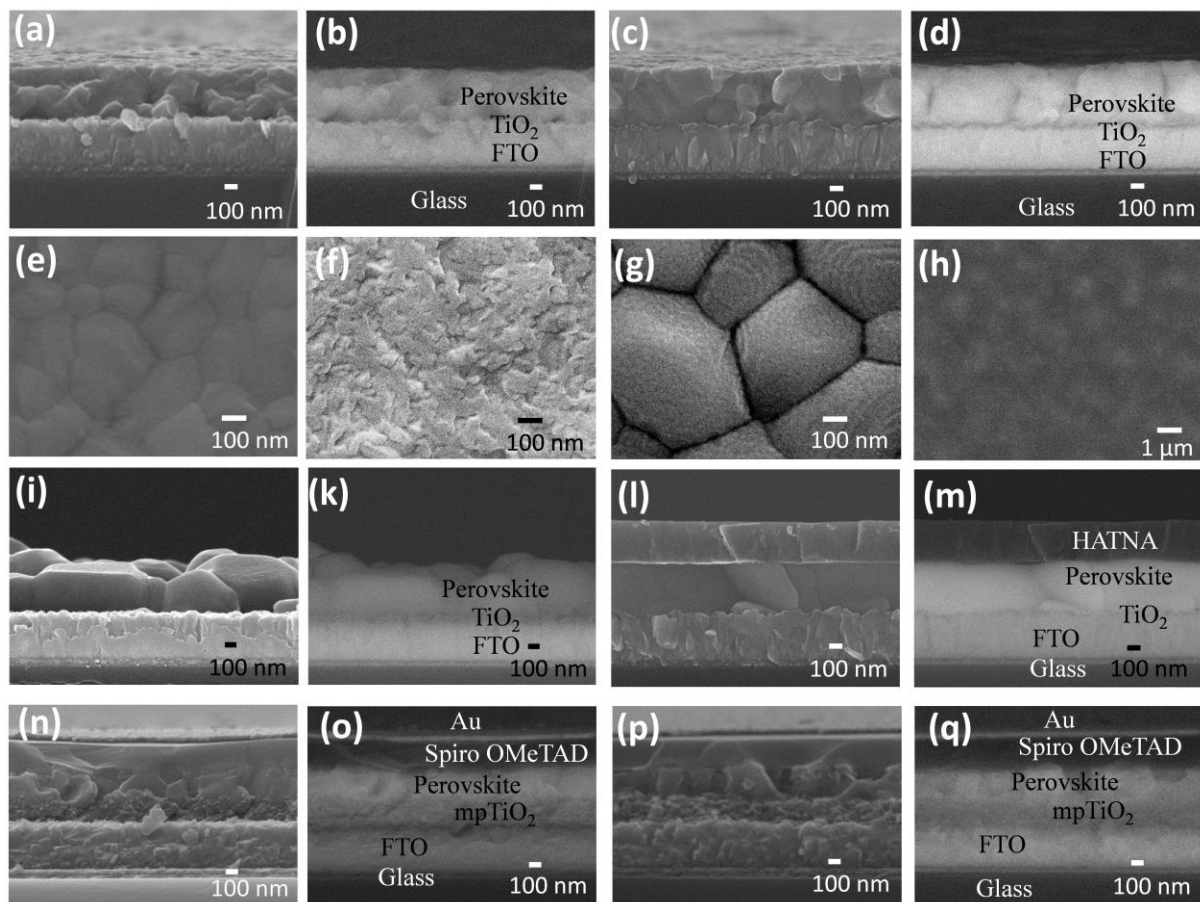
Figure S7. SEM micrographs obtained with secondary electrons (SE) and with backscattered electrons (BE). BE are highly sensitive to the composition, showing with a clear color the

28

areas containing heavy atoms as Pb, while organic compounds present a darker contrast. PS

film prepared with chlorobenzene anti-solvent **(a)** cross section (SE), **(b)** cross section (BE)

and **(e)** top view. PS+DCL97 film prepared with chlorobenzene anti-solvent **(c)** cross section

(SE), **(d)** cross section (BE) and **(f)** top view. PS film prepared with diethyl ether anti-solvent

(i) cross section (SE), **(k)** cross section (BE) and **(g)** top view. PS+HATNA film prepared

with diethyl ether anti-solvent **(l)** cross section (SE), **(m)** cross section (BE) and **(h)** top view.

Complete device with glass/FTO/compact TiO_2/mesoporous (ms) TiO_2 /PS/spiro-

OMeTAD/Au configuration prepared with diethyl ether anti-solvent **(n)** cross section (SE),

(o) cross section (BE). Complete device with glass/FTO/compact TiO_2/mesoporous (ms) TiO_2

/PS-HATNA/spiro-OMeTAD/Au configuration prepared with diethyl ether anti-solvent **(p)**

cross section (SE), **(q)** cross section (BE).

S8. Open Circuit Voltage Decay.
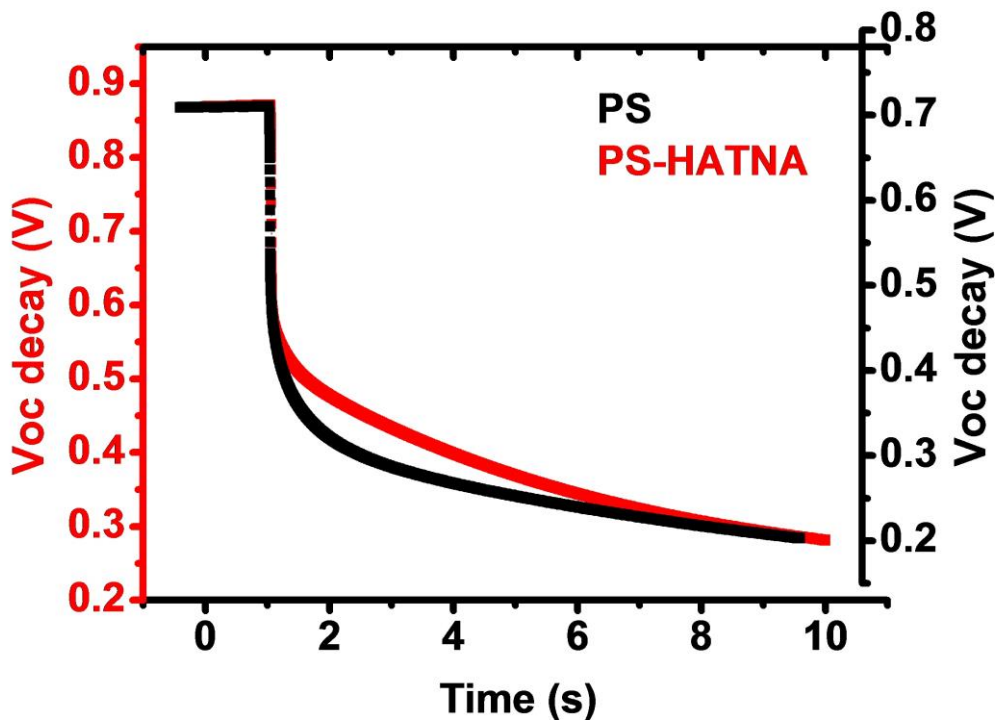
Figure S8. Voc decay measured at 0.09 sun.

S9. Photoluminescence mapping of perovskite film with additives.
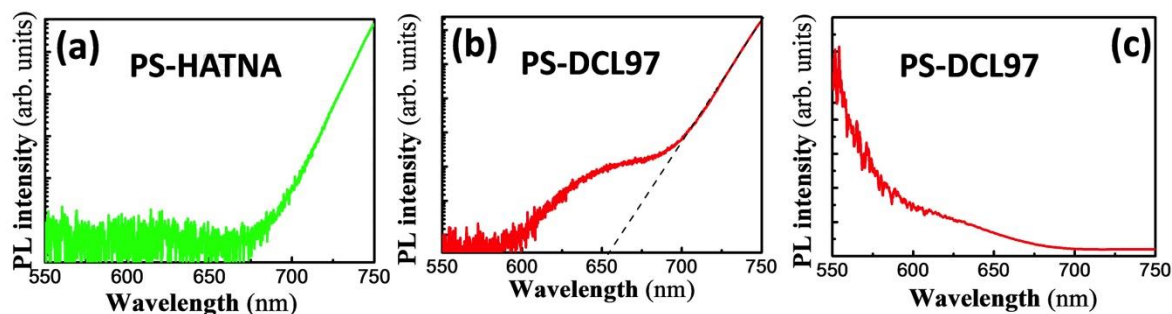
Figure S9. PL spectra for λ_{exc}=533 nm excitation wavelength of **(a)** PS-HATNA and **(b)** PS-DCL97. This λ_{exc} can just excite PS in the case of PS-HATNA and just the PS PL queue is observed at 700-750 detection wavelengths, λ_{dec}. The detected wavelengths have not been extended to longer wavelengths in order to avoid the saturation of the detector. In the case of PS-DCL97 both PS and DCL97 are excited with λ_{exc}=533 nm, and in addition to the PS PL queue a shoulder in the perovskite spectra at λ_{dec} =600-700 nm can be observed in (b). Consequently in order to discriminate the PL produced by PS or by DCL97 PL maps are recorded for different λ_{dec}. Figure 3f shows the integrated PL for λ_{dec} =700-750 nm that takes only into account the PL from the PS, see (b).In order to obtain the PL coming from DCL97, the PS contribution, obtained from the linear fitting of the PS PL queue (dashed line in b), is subtracted to the PL spectra in (b) obtaining the bare contribution of DCL97 plotted in **(c)**. Figure 3d shows the integrated PL for λ_{dec} =600-650 nm, after removing the PS contribution, that takes only into account the PL from the DCL97.

S10. Photoluminescence mapping of PS-DCL97 sample at an alternative position than the reported in Figure 3.
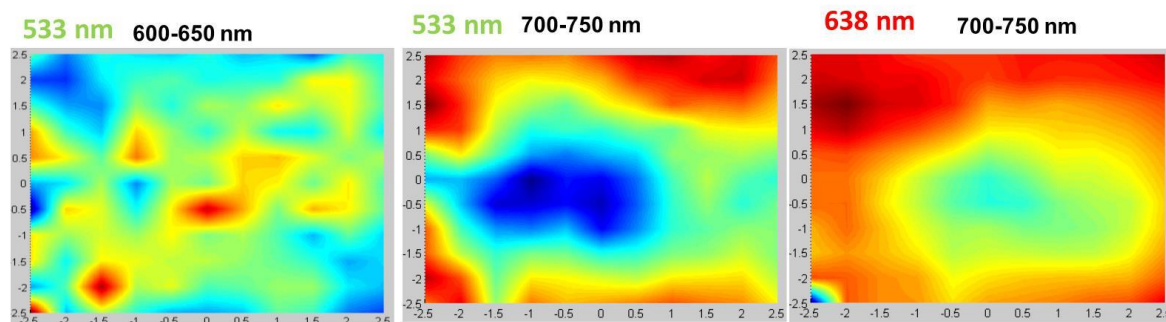
Figure S10. Photoluminescene intensity map of a sample of perovskite with DCL97 additive, excitation wavelength, λ_{exc}, and the range of detected wavelengths, λ_{det}, are indicated in each map with green-red color and with black color respectively. **a)** PL from DCL97, where PL from perovskite has been subtracted, see Figure S9, for further details. **b)** and**c)** PL from perovskite, see Figure S9, for further details, for two different λ_{exc}. Vertical and horizontal scales for the maps are in μm.

S11. Solar cell stability during impedance measurement.
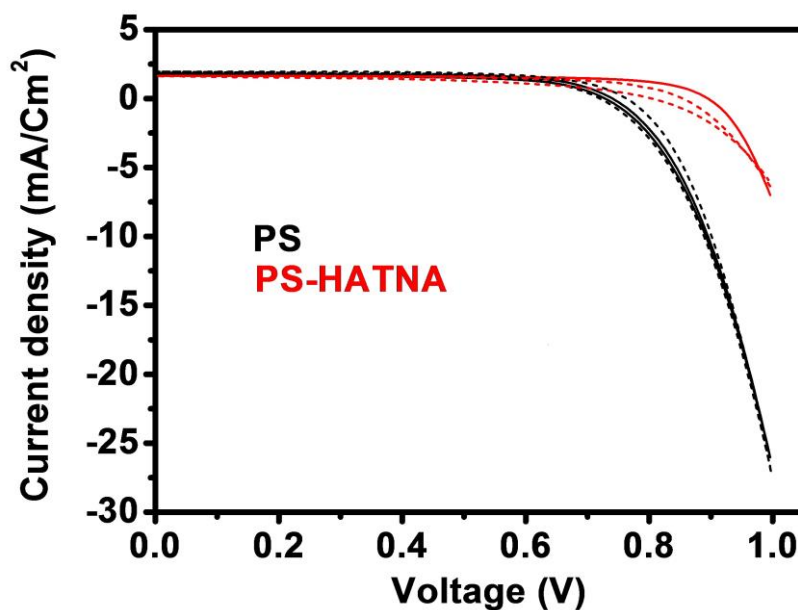
Figure S11. J-V curve at 0.09 sun of devices based on PS and PS-HATNA absorbers before

(solid line) and after Impedance measurement (dash line).

Supporting Information
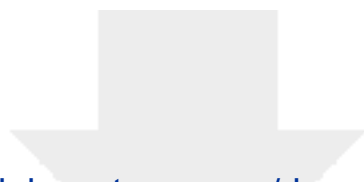
Click here to access/download

Supporting Information
16 10 14 PS+Organic_rev_Changes Highlighted.docx
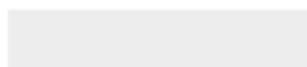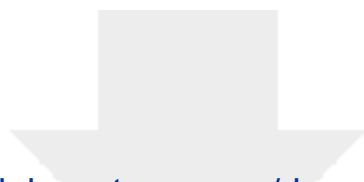
Production Data

Click here to access/download
Production Data
16 02 PS+Organic.rar